Tellus (1992), *44A*, 339–355

Multicell stage of the Munich storm of 12 July 1984: a numerical study

By ROGER BRUGGE[1], *Imperial College, London SW7 2BZ, England*, and MITCHELL W. MONCRIEFF, *National Center for Atmospheric Research*[2], *Boulder, Colorado 80307-3000, USA*

(Manuscript received 9 April 1990; in final form 24 March 1992)

ABSTRACT

The multicell stage of the Munich hailstorm is investigated using a three-dimensional, non-hydrostatic mesoscale model. During this stage, the storm developed in a wind profile that had little directional shear yet an extensive series of two-dimensional numerical experiments could not produce a self-sustaining and realistic convective system. The modelled storm is a multicellular, three-dimensional system featuring right-flank development of new cells. It is constituted of two principal flow branches, namely, an intense updraught that travels at the speed of a mid-level steering current and a weak downdraught. A mid-level relative inflow overtakes the storm from the rear but undergoes unsaturated descent of only about 100 mb, fails to establish the classical downdraught associated with mid-latitude storms, and exits ahead of the storm. Weak, shallow downdraughts originate beneath an inversion and from ahead of the storm. Viewed in a cross section parallel to the direction of storm motion, trajectory analyses show that the cold pool is fed by two types of shallow downdraught, namely a gravity or solitary wave undergoes minimal vertical displacement and an overturning jump that causes substantial evaporative cooling despite its small vertical displacement. A density current circulation fails to form in this plane but one does develop in the perpendicalur section and its interaction with the convergence field and vertical shear causes secondary cell initiation at right angles to that found in multicell squall lines.

1. Introduction

On 12 July 1984, between 1600 and 2000 GMT (1800 and 2200 CEST), parts of southern Bavaria in southern Germany were devastated by a hailstorm of exceptional severity that caused extensive damage to buildings and crops (Höller and Reinhardt, 1986). The city of Munich suffered the highest degree of destruction. Total insurance claims equivalent to $500 million were submitted as a result of damage by hailstones that were typically 5–6 cm, with some as large as 9.5 cm, in diameter (Berz, 1984). Munich lay in the middle of a hail swath approximately 250 km in length and 5–15 km in width, and precipitation totals of up to 40 mm were recorded in the Munich area where surface temperature falls of 5 to 7 deg C were observed. The storm had a complex life cycle because it evolved from a multicell, through a supercell and by late evening it developed into a mesoscale convective complex (MCC; Maddox, 1980) that travelled northeastwards towards Czechoslovakia and Poland. Heavy rainfall was reported from these countries (65 mm in Svatouch, Czechoslovakia and 42 mm in Warsaw, Poland) before the system moved towards Leningrad, USSR and dissipated.

The synoptic-scale thermodynamic and wind profiles are well known to have an important effect on convective storm movement, intensity and dynamical structure. The modelled storm environment had strong vertical shear in low levels with weak shear aloft that has been shown to be conducive to two-dimensional, long-lived convection

[1] Current affiliation: Department Meteorology, University of Reading, Reading, Berks, RG6 2AU, England.

[2] The National Center for Atmospheric Research is funded by the National Science Foundation.

(Thorpe et al., 1982; Rotunno, et al., 1988; Crook and Moncrieff, 1988; Fovell and Ogura, 1989; Lafore and Moncrieff, 1989). It was thought a priori that the Munich storm might be dynamically similar to this type of convection. In retrospect, the storm evolution was found to be much more complex. Extensive two-dimensional simulations were unsuccessful in reproducing the observed storm behaviour. The modelled storm in a three-dimensional entity despite the almost unidirectional ambient wind profile.

2. Observations and the synoptic situation

The synoptic situation prior to the development of the storm has been discussed in detail by Heimann and Kurz (1985) and Kurz (1985). On 11 July 1984, southern and eastern parts of Germany were under the influence of a hot and dry air mass of Saharan origin that had moved into central Europe between a weak low over France and Spain and a ridge that extended from the Mediterranean to the Baltic Sea. The daytime maximum temperature in Munich reached 37°C. The temperature at the Hogenpeissenberg (977 m a.m.s.l.) reached 32.4°C, the highest value recorded in over 200 years. This was due to a foehn along the northern edge of the Alps. During the evening a low pressure area and an embedded cold front approached Bavaria from the west. Thunder was heard but the front was very weak by the time it reached eastern parts of Bavaria, causing only a wind-shift from south to northwest at Munich and partial stratocumulus cloud cover. As pressure rose later in the night, thunder activity in north and west Bavaria ceased and cooler, moister air moved into Bavaria as far south as the Alps, causing a pronounced inversion along the frontal zone. On 12 July heat lows formed over the Alps between the ridge over France and the quasi-stationary anticyclone over the Mediterranean. The study of Heimann and Kurz (1985) suggested a slow ascent (up to 500 mb) of air over southern Germany that was linked to warm air advection in the lower troposphere.

The first precipitating cells were observed by radar over the Bernese Oberland at 1235 GMT (Höller and Reinhardt, 1986), their formation probably assisted by orographically-induced lifting, although it took longer to destabilize air on the northern flank of the Alps. Fig. 1 shows the temperature and moisture profiles at Munich for 0000 GMT and 1200 GMT on 12 July. The 0000 GMT sounding shows a hot and dry air mass at all levels except near the surface where the effect of the cold frontal passage is evident. As the colder and moister air crossed Bavaria, cooling of up to 12°C in a mixed layer 2200 m deep occurred by noon. At the top of this layer, the 1200 GMT sounding shows a pronounced 4 deg C temperature inversion that formed part of the sloping frontal zone. The lapse rate was stable with respect to convection generated by surface heating so only suppressed shallow cumulus developed in the morning. This probably accounted for the absence of an early prediction of storm development, but was conducive to the generation of substantial available potential energy for subsequent deep convection.

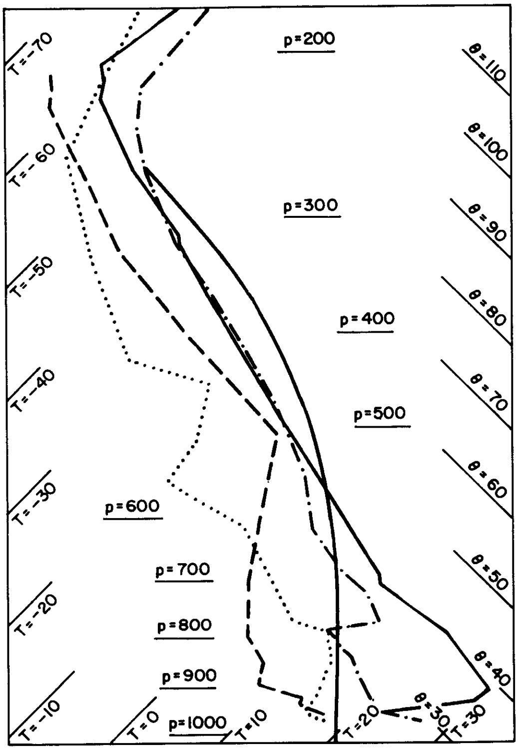

Fig. 1. Temperature soundings made at Munich on 12 July 1984. 0000 GMT temperature (full) and dew point (broken). 1200 GMT temperature (broken-dotted) and dew point (dotted). The $\theta_w = 20$°C moist adiabat is also shown by a full line.

3. Numerical model

The numerical model is the non-hydrostatic pressure coordinate model of Miller and Pearce (1974) with more recent changes as described in Dudhia and Moncrieff (1989). The model does not include orography in the lower boundary condition. The horizontal domain of the model is 100 km × 100 km with a depth of 850 mb and surface pressure of 960 mb. Grid lengths of 2 km in the horizontal and 50 mb in the vertical were used. The horizontal resolution is barely adequate and a grid length of 1 km would be preferable.

The sub-grid scale diffusion used in the momentum equation is of the form $K\nabla^2 v'$, where v' is a velocity component. In the thermodynamic and moisture equations diffusion is $K\Delta^2\nabla^2\phi'\,|\nabla^2\phi'|$, where ϕ' is a perturbation from the initial state and Δ is a grid length. The effective diffusion coefficient is given by $K\Delta^2\,|\nabla^2\phi'|$. Note that the diffusion is applied only to the perturbations and not to the mean fields. The values of the horizontal diffusion coefficient (K_h) used were 8×10^3, 6×10^2 and $6\times10^3\ \mathrm{m^2\,s^{-1}}$ for velocity, potential temperature and moisture, respectively. The values of the vertical diffusion coefficient (K_p) were 2.5×10^3, 1.25×10^2 and $1.25\times10^5\ \mathrm{m^2\,s^{-1}}$ for velocity, potential temperature and moisture, respectively. Thus for the thermodynamic and moisture perturbations the effective diffusion coefficient is K times a value whose magnitude is roughly that of the field being smoothed; this value is O(1) for perturbation potential temperature and $O(10^{-3})$ for moisture perturbations specified in the model in units of g/g. Consequently, the effective magnitudes of diffusion are similar in the momentum and thermodynamical equations.

The model does not take account of the ice

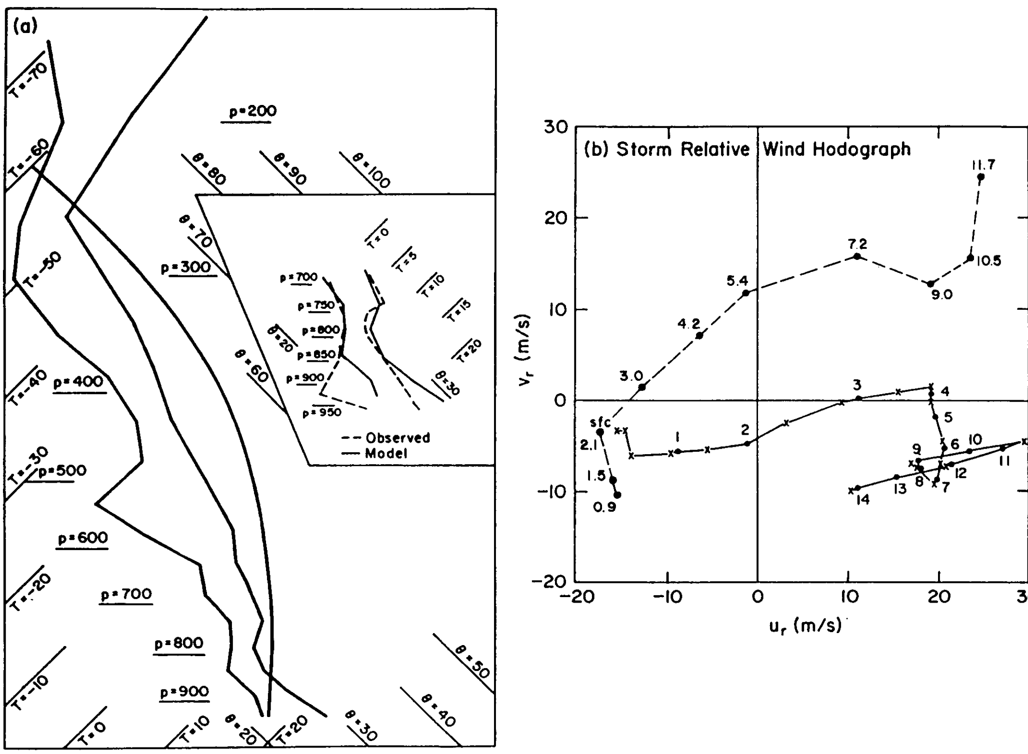

Fig. 2. Initial conditions, derived from the Payerne 1200 GMT sounding, used in the simulation. (a) Temperature and moisture; (b) relative wind profile in $\mathrm{m\,s^{-1}}$. The 1800 GMT wind profile at Munich is shown by the broken-line hodograph. The inset in (a) shows the observed Payerne temperature and moisture conditions (broken lines) in the lower atmosphere. The model winds have been rotated clockwise through 45° and are relative to an estimated cell velocity $v_c = (15.3\ \mathrm{m\,s^{-1}}, 4.5\ \mathrm{m\,s^{-1}})$ in the rotated frame. The numbers denote heights above ground level (km).

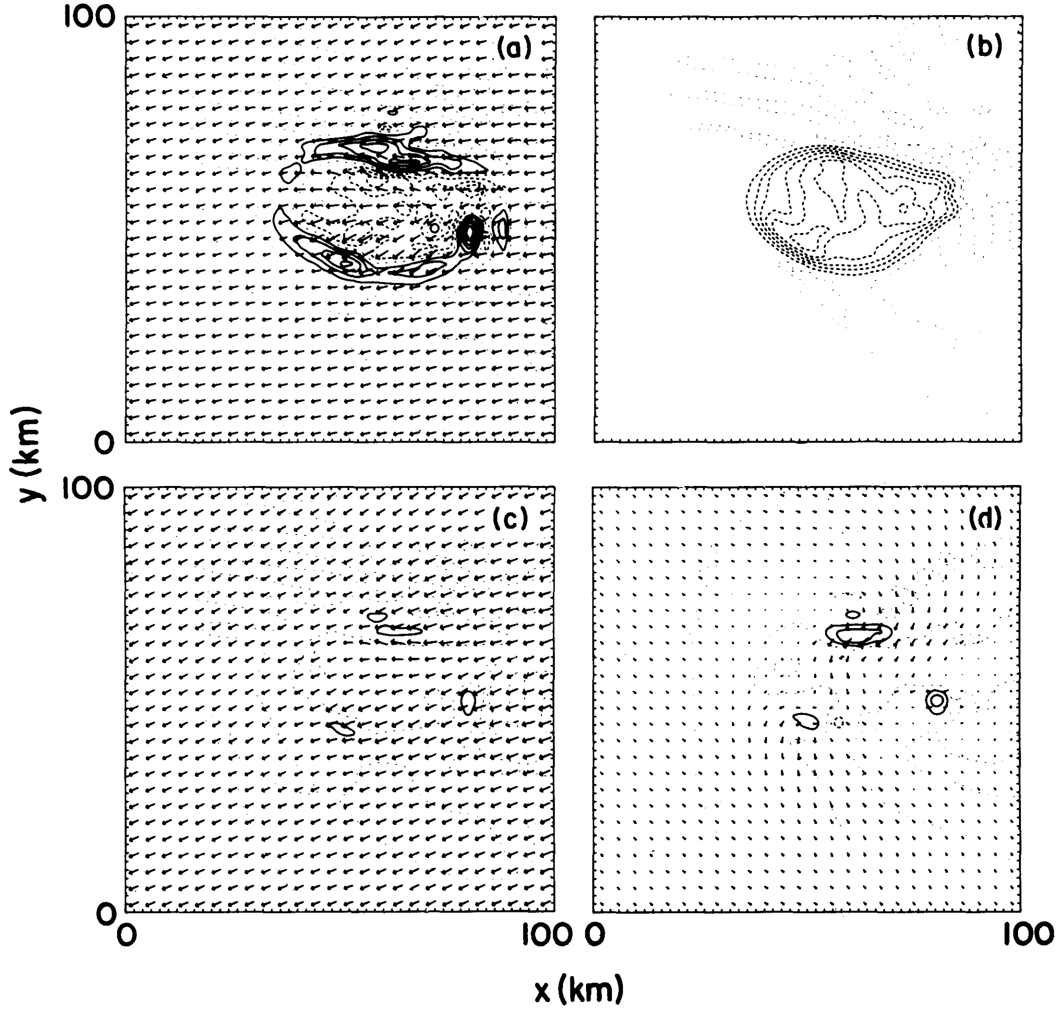

Fig. 3. Fields at $t = 60$ minutes. (a) 935 mb winds and the horizontal convergence with contour interval $10^{-3}\ s^{-1}$ (broken lines indicate divergence); (b) 935 mb temperature deviation with contour interval 1.0°C; (c) 885 mb winds; (d) 735 mb winds. Updraughts (full) and downdraughts (broken) are drawn for speeds in excess of 2 m s^{-1}, contour interval 2.0 m s^{-1}; (e) 735 mb height perturbation with contour interval 1.0 m. Positive (negative) values shown by continuous (broken) lines; (f) Surface rainfall rates with contours drawn for 0.1, 15, 30, and 45 mm h^{-1}; (g) 735 mb cloudwater and (h) 335 mb cloudwater, with contours drawn for 0.1, 0.5 and then every 0.5 g kg^{-1}. In these and later horizontal plots the domain is 100 km × 100 km with tick marks every 2 km.

phase in the microphysical parameterizations. From the observed size of the hailstones in the Munich area the model parameterization of rainwater fallspeeds should include the effects of hail, allowing precipitation to more readily escape from the updraughts. The terminal fallspeed (V_t) expression used is $V_t = \alpha l_r^{0.2}$, where l_r is the rainwater content in units of g kg^{-1}. The value of $\alpha = 10.0$ m s^{-1} was used to parametrize of the effect of a weighted average of rain and hail in a simple way (Miller, 1978). However, this parameterization cannot account for vertical variations due to mixed precipitation types such as rain-hail below the melting level, graupel-hail in intermediate levels or graupel-ice in the upper levels.

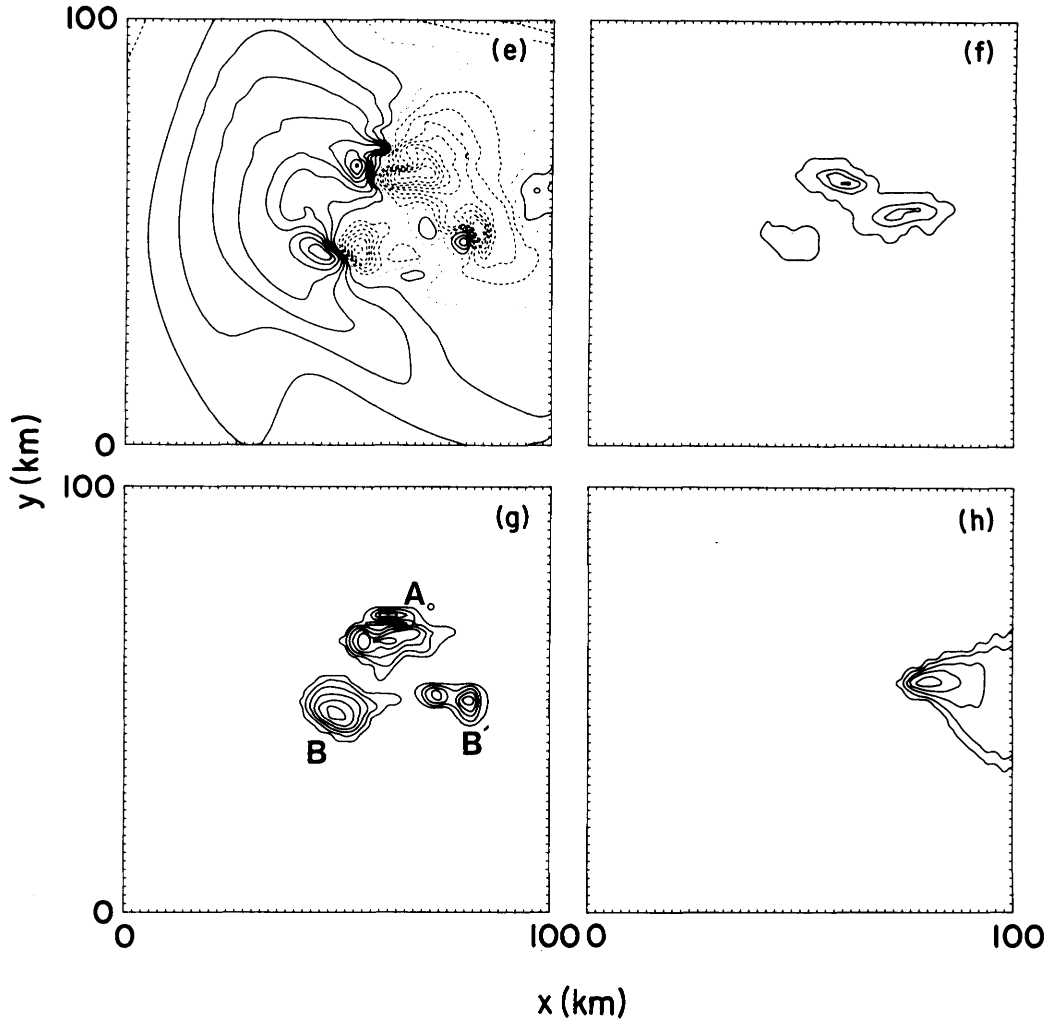

Fig. 3 (cont'd)

Fig. 2 shows the observed temperature and wind data used to initialise the simulations, based on the 1200 GMT radiosonde ascent from Payerne. The model winds were obtained from the observations by clockwise rotation through 45° so that the transformed surface wind had an approximately east–west direction. The model-calculated cell velocity $v_c = (15.3 \text{ m s}^{-1}, 4.5 \text{ m s}^{-1})$ was subtracted in the rotated frame to ensure that the storm remains almost stationary in the model domain. The cell velocity compares with an observed travel speed for the storm over Munich of 16.6 to 19.4 m s^{-1} (Heimann and Kurz, 1985). Unless otherwise stated, all bearings and directions are relative to this rotated storm-relative reference frame.

The initial temperature and moisture profiles used in the simulation were taken from observations (interpolated to the required pressure levels) except in the planetary boundary layer where it was found necessary to increase the equivalent potential temperature to expedite penetration of the 735 mb inversion. Note that the model cannot adequately resolve this inversion due to the 50 mb vertical grid length. Numerous test simulations were performed with and without an augmented boundary layer energy (and various distributions and strengths of heat and moisture sources/sinks at mid- and low-levels to initiate convection). The results unambiguously indicated the need for a substantial increase in the surface buoyancy to sustain convection once the imposed initial source/sink was switched off. The complex issue of convection initiation in the proximity of orography cannot be studied with this model so a sophisticated initiation is beyond the scope of this study. A simple and commonly-used heat source initiation was used to generate the low-level conditions necessary for the convection initiation. A heat source with an amplitude of 0.01 K s^{-1} was applied during the first 30 minutes of the simulation over 11×6 gridpoints (an area of 264 km^2) in the x and y directions and between 785 and 935 mb. The region of heating was held stationary with respect to the ground-relative (observed) winds and therefore translated to the southwest at the velocity v_c in the frame of reference moving with the storm.

4. Structure of the modelled storm system

The first few tens of minutes of the simulation were dominated by the effects of the heat source. Thereafter, secondary cells were spawned as a result of locally strong, boundary layer convergence caused by the cold air outflows from pre-existing convective cells. Dynamical analysis was performed on one of these, namely, cell B (see Fig. 3g).

4.1. Initial development

The initial development consisted of a vigorous updraught generated by the heat source. After 15 min, strongly convergent boundary-layer winds and the conditionally unstable air above the inversion generated vertical velocities up to 11 m s^{-1} in the 635 to 735 mb layer. Deep convection developed rapidly, with cloud base at about 835 mb, and after 30 minutes surface rainfall rates of up to 180 mm h^{-1} were attained.

The low-level temperature perturbation features the development of a cold surface pool generated by an evaporatively-cooled storm outflow that grew in depth and horizontal extent between 30 and 60 min, mainly in a westward direction as a consequence of the surface wind velocity. The 935 mb horizontal winds at 60 minutes (Fig. 3a) show convergence on the north and south flanks of the pool, which has a temperature deficit up to -6°C at 935 mb (Fig. 3b) and -4°C at 885 mb. The cold pool coincided with the formation of a high pressure region at 935 mb.

Low-level ascent exists on the northern and southern flanks of the pool (Figs. 3c and d), the northern convergence zone being the original, source-induced region that declines in strength. The 735 mb height perturbation field (Fig. 3e) shows a high/low couplet with an axis that is approximately in the direction of the ambient shear. Surface rainfall at 60 minutes occurs in an elongated east–west strip (Fig. 3f) and the maximum rainfall rate decreases to 47 mm h^{-1} beneath the original cell A. There is already surface precipitation from the cell on the southwestern flank of the pool with instantaneous rainfall rates of up to 12 mm h^{-1} at 60 minutes (cell B, shown in Fig. 3g), while a short-lived cell (B′) exists to the east of the pool. Comparing Figs. 3g and h, the cloud shows a prominent eastward (downshear) tilt with height. The downdaught lies to the southeast of the updraught.

4.2. Secondary cell development

The convective activity on the northern flank declined between 60 and 120 min but cloud formed on the southeastern flank of the cold pool. This

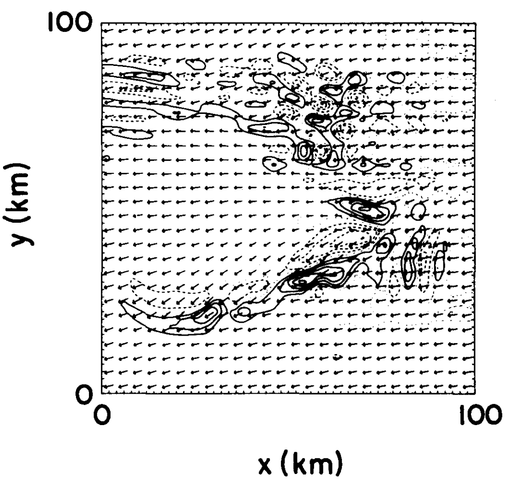

Fig. 4. 935 mb horizontal wind vectors at $t = 105$ minutes and horizontal convergence with contour interval 10^{-3} s^{-1}. Broken lines indicate divergence.

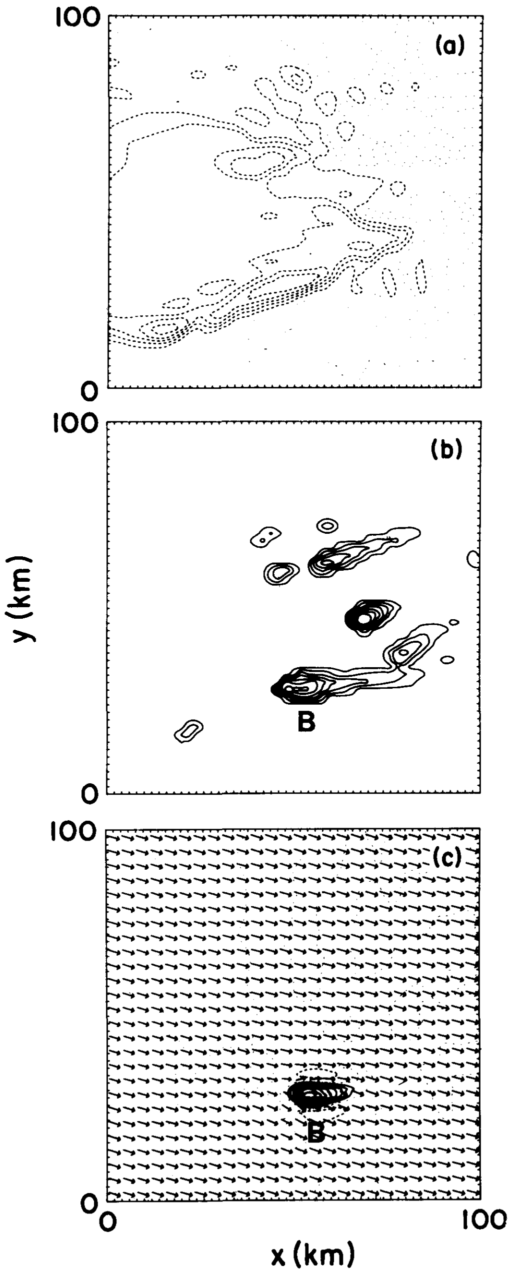

Fig. 5. Fields at $t = 120$ minutes: (a) 935 mb temperature deviation with contours drawn at intervals of 1°C. Negative (positive) values shown by broken (broken-dotted) lines; (b) 635 mb cloudwater content with contours drawn for 0.1, 0.5 and then every 0.5 g kg^{-1}; (c) 435 mb winds with full (broken) lines indicate ascent (descent). Vertical velocity contours drawn every 2.0 m s^{-1}.

occurred slowly at first then developed rapidly between 105 and 120 min as the updraught suddenly accelerated. By 105 minutes strong horizontal boundary layer convergence exists on the southern flank (Fig. 4). By 120 min, the surface rainfall rate increased with values up to 98 mm h^{-1} on the southern flank. The region of cloud formation is horseshoe-shaped with the open end to the westsouthwest. The overall structure consisted of a family of cells, rather than a single large mass of cloud, overlying the edge of the cold pool (Figs. 5a, b). The deepest cell (B) overlies the southern edge of the cold pool, with vertical velocities as large as 17 m s^{-1} (Fig. 5c). This cell and its associated intense surface precipitation is the dominant feature between 120 and 150 min, enhancing the cold surface air on the southern edge of the original cold pool (Fig. 5a). The 150 minute fields in Fig. 6a show the development of a new cell near the southwestern corner of the domain, although its behaviour is probably influenced by the proximity of this boundary. Nevertheless, the history of the simulation and the enhancement of the cold pool is conducive to continued convective development.

Secondary cells developed on the southern flank of the cold pool, at a location that lies on a bearing of approximately 210° from the parent cell in the model frame of reference. The lifetimes of the successive secondary cells exceed two hours. Similar development of right-moving cells were identified using radar and Meteosat imagery by Höller and Reinhardt (1986). This demonstrates that the multicell nature of the simulated convection during this evolutionary stage of the storm complex is realistic.

Previous modelling experiments have produced the right-flank growth, right-moving cells and splitting of multicell storm systems. Thorpe and Miller (1978) demonstrated these tendencies in two experiments. The initial wind profile in their first experiment (A) featured a small change of wind direction with height in low levels, and secondary cells developed to the right of their parents, reminiscent of the simulation herein. Their second simulation (B), in a more highly sheared environment, demonstrated distinctive redevelopment (or splitting) both to left and right of the parent cell. The wedge-shaped cold air pool in case B compares with the one produced herein. Klemp and Wilhelmson (1978) also obtained splitting

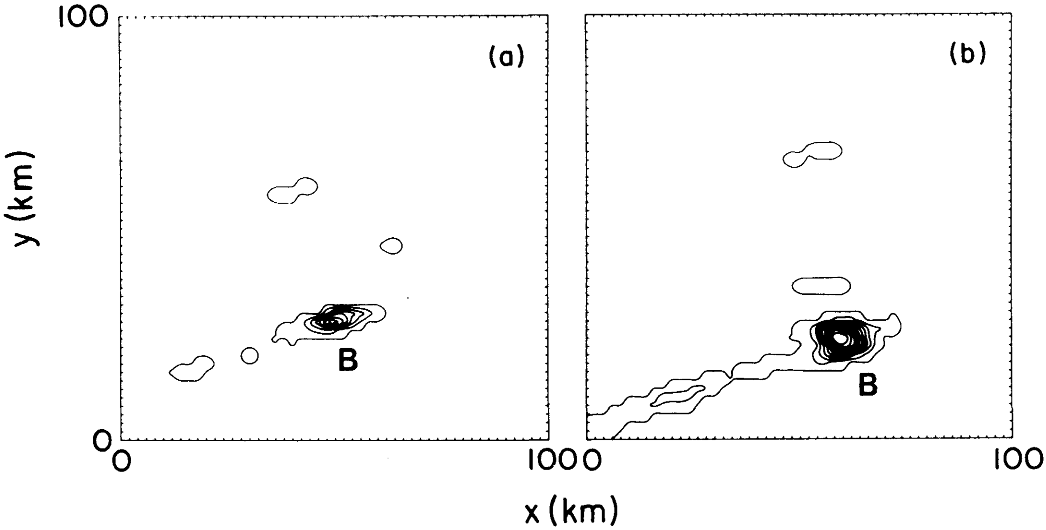

Fig. 6. Rainfall rates at: (a) 120; (b) 150 min. Contours drawn for 0.1, 15.0 mm h^{-1} and then every 15 mm h^{-1}.

left- and right-moving cells in their numerical experiments. These studies emphasised the importance of the turning of the wind with height in promoting right-moving and multicell behaviour, although neither study suggested that this should be a necessary condition. A splitting and right-moving behaviour is found herein, but an important difference arises through the form and intensity of the downdraught. As demonstrated in the subsequent trajectory analysis, the downdraughts in the Munich storm simulation were weak and originated ahead (upstream) of the updraught. This is in contrast to the strong, rear-to-front downdraughts in the Thorpe and Miller (1978) and Klemp and Wilhelmson (1978) studies.

Multicell, right-moving behaviour is evident in the rainfall rates at 120 and 150 min and accumulated rainfall between 60 and 150 min, shown in Figs. 6 and 7, respectively. Allowing for ground-relative translation, cell B would yield an average of 9 mm of precipitation over a storm track about 14 km wide between 120 and 180 min of simulation time with a maximum of about 25 mm in any location. Cell development implies that the orientation of the precipitation bands in the rotated model frame is 240–060°. The absence of an ice-phase in the model means that only a qualitative account of the cloud microphysical structure is possible so the dynamical structure of the storm is the focus of attention.

4.3. Updraught structure

A convective Richardson number was defined by Moncrieff and Green (1972) as $\mathrm{Ri} = \mathrm{CAPE}/\frac{1}{2}U_0^2$, where CAPE is the convective available potential energy and $\frac{1}{2}U_0^2$ is the specific kinetic energy of the near-surface relative inflow. The initial sounding in Fig. 2a gives CAPE ≈ 1200 J kg^{-1} and from the wind profile in Fig. 2b, $U_0 \approx 16$ m s^{-1} layer, so $\mathrm{Ri} \approx 10$. In constant vertical shear a Richardson number of this magnitude is commensurate with unsteady convection (Moncrieff, 1978). Weisman and Klemp (1984) use a somewhat different definition of the convective Richardson number, namely $R = \mathrm{CAPE}/\frac{1}{2}(\Delta U)^2$, where ΔU is the environmental shear between 500 m and 6 km. Since $\Delta U = 35$ m s^{-1} it follows that $R \approx 2$, a magnitude that favours multicell, splitting storms. Notably, observations and simulations both show this behaviour with the cells at the southern side of the cold pool being favoured.

An east–west vertical section through cell B show the pronounced downshear (southeastward) tilt of the storm updraught (Fig. 8a, b). In Fig. 8c, the primary features of the relative flow are the overturning updraught, the strong inflow from the rear that remains elevated and fails to form the rear-to-front type of downdraught that is typical of severe mid-latitude storms, and the low level downdraught inflow from ahead of the storm.

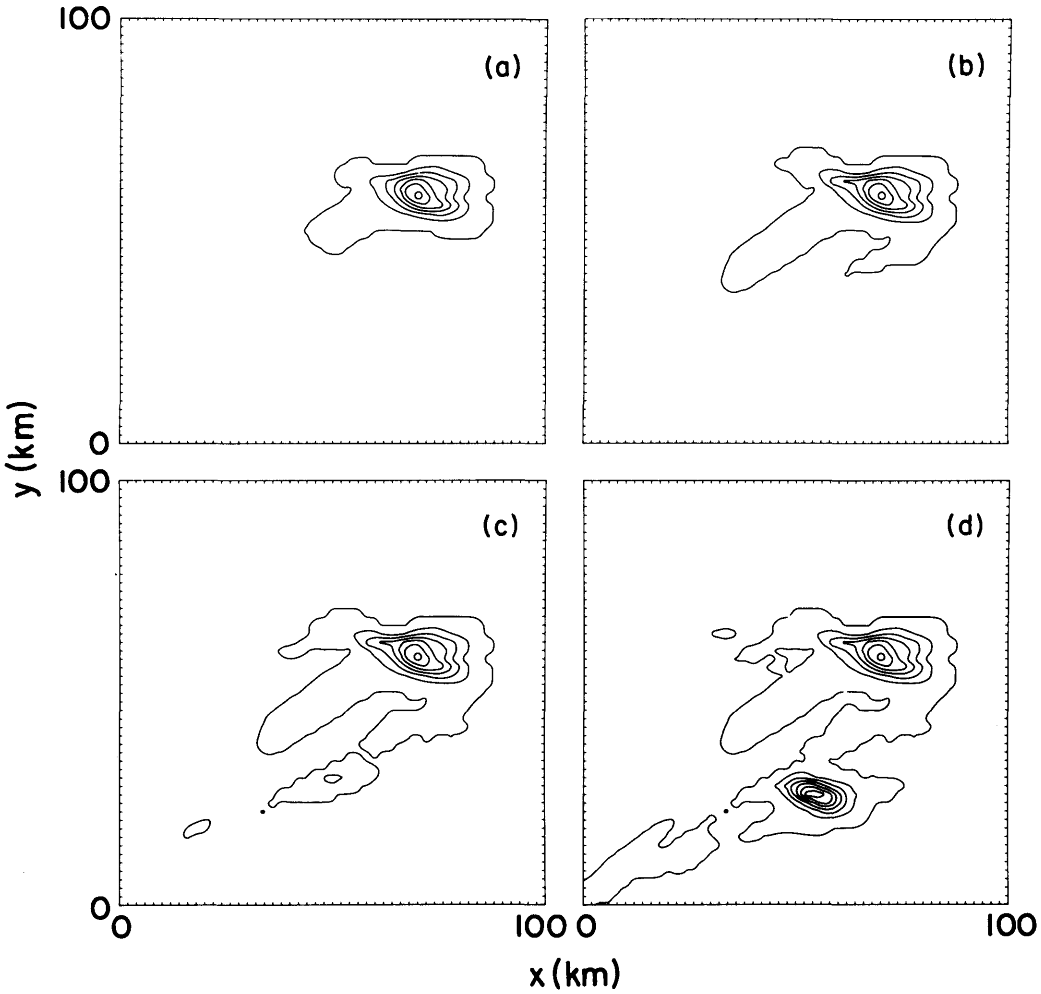

Fig. 7. Accumulated rainfall totals after: (a) 60 min; (b) 90 min; (c) 120 min; and (d) 150 min. Contours drawn for 0.1, 10.0 mm and then every 10 mm.

A trajectory analysis of airflow through cell B was undertaken to elucidate the storm-scale dynamics. Fig. 9 shows selected trajectories through this cell and indicates two updraught branches. Fig. 9 shows selected trajectories through this cell and indicate two updraught branches. The dominant "steering level" branch originates in the low-level flow from the northeast and outflows in a southeastward direction between 270 and 370 mb. A second weak branch originates between 750 and 880 mb, splits and leaves the updraught between 330 and 470 mb. An additional weak ascent originates from the mid-level westerly flow between 510 and 450 mb and could be due to the entrainment of environmental air by mixing with the principal updraught branches.

A conceptualisation of the structure of the airflow relative to the long-lasting ($\sim$2 hours) storm cells is shown in Fig. 10. The steering-level updraught branch (Moncrieff, 1981) that moves at the speed of the ambient flow at a steering level is a dominant feature. Two weak descending regions are shown: one is associated with the low-level downdraughts and the other with an unsaturated

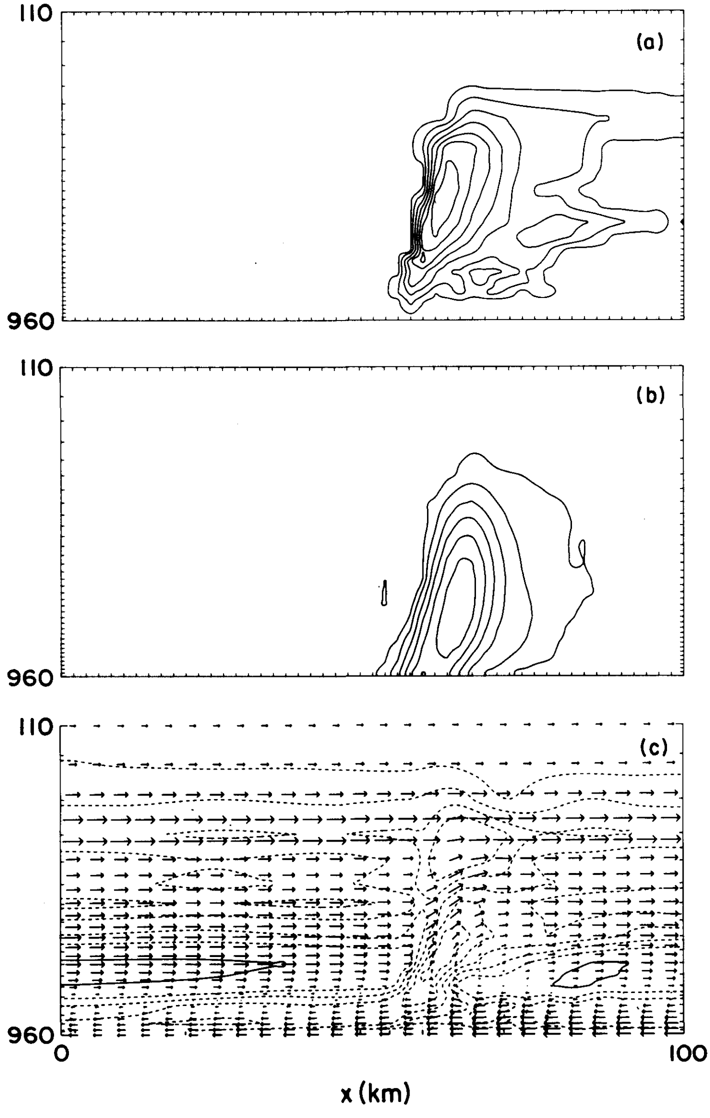

Fig. 8. Fields at 150 min: East–west sections of (a) cloudwater content; (b) rainwater content, both with contours drawn for 0.1, 0.5 and then every 0.5 g kg^{-1}; (c) East–west sections through the model at 150 minutes showing the winds normal (contour interval of y-velocity is 2 m s^{-1}) and parallel (arrows) to the section.

descent region in mid-troposphere. The latter has a negligible dynamical impact on the storm and is the midlevel inflow from the rear, identified in Fig. 8c. This inflow fails to establish an overturning downdraught, that is the classical and primary type of cloud-scale descent often found in severe storms.

4.4. *Downdraught structure*

The role of cold air pools has long been recognised to be of primary importance in convection initiation and development. More recently, the role of strong lower-tropospheric vertical shear and its interaction with the cold air pool was studied by Thorpe et al. (1982) and Rotunno et al.

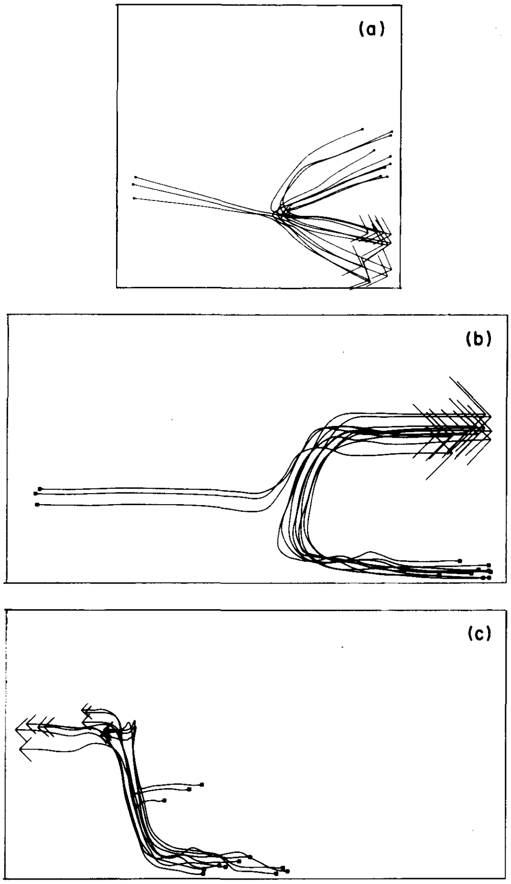

Fig. 9. Air trajectories of air passing through cell B between 80 and 180 min. (a) Plan-view, (b) west–east projection (west to left) and (c) north–south projection (south to left).

(1988), respectively. However, in the Munich storm simulation the airflow, convergence and vorticity production in a plane parallel to storm travel are weak. Front-to-rear moving air in the wavelike and jump downdraughts is quite distinct from the strong, rear-to-front downdraughts and classical density currents.

Fig. 8c shows the descending air underlying a tilted updraught. The descent speeds are between 0.4 and 2.0 m s^{-1} at pressure levels of 610, 810 and 910 mb. There is no evidence of a robust downdraught although a temperature deficit of -7°C within a significant proportion of the cold pool has been produced. The relative flow at ground level in a plane parallel to the storm travel direction fails to form a density current circulation. The downdraught trajectory analysis (Fig. 11) indicates that air does not descend more than 150 to 200 mb. The downdraughts occur within a region of weak, longer-lived descent southeast and southwest of the updraught. The air that reaches the surface by descending through the rain area originates from beneath the inversion in the 750–930 mb layer ahead of the cells, demonstrated by θ_w analyses (not shown).

The weakness of the downdraught and the wavelike airflow through the cold pool are both somewhat unusual in severe mid-latitude storms. In squall lines the component of the cold air outflow in the direction of travel commonly has a surface stagnation point behind which there may be flow reversal — a gravity or density current. Herein, the low-level inflow to the cold air pool originates totally from ahead of the storm. A trajectory analysis of the downdraught was undertaken to study its dynamical structure. Fig. 11

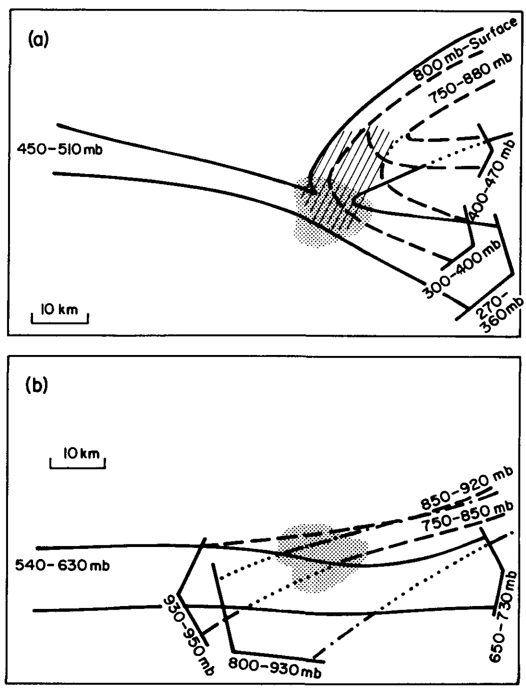

Fig. 10. Schematic plan views for air trajectories; (a) ascent, (b) descent. Stippling denotes region with a rainfall rate in excess of 15 mm/h at 150 min. Hatching indicates principal ascent region at 150 min. Pressure levels of the inflow and outflow are indicated.

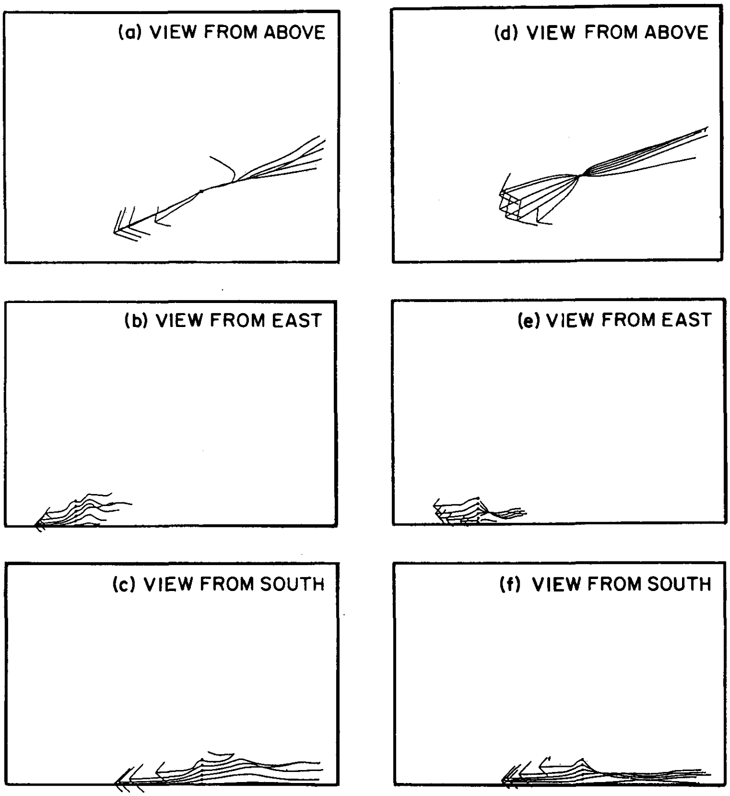

Fig. 11. Selection of forward (150–180 min) and backward (150–80 min) trajectories passing through the cold air pool. Note that in plates (a)–(c) trajectories do not overturn unlike those in plates (d)–(f).

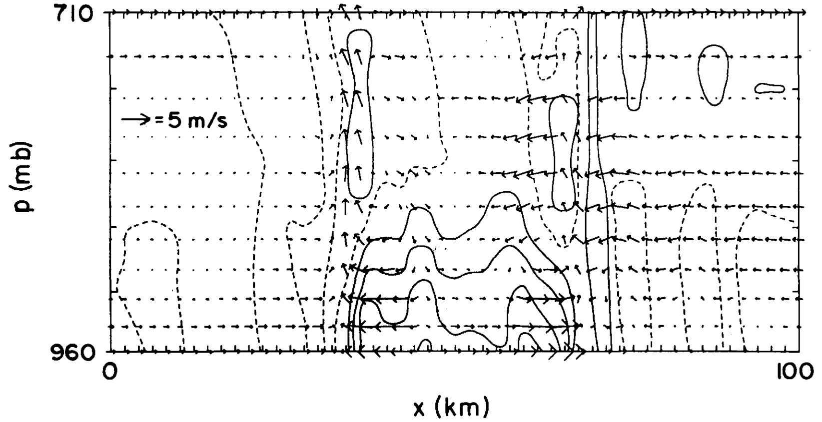

Fig. 12. North–south vertical cross section at 90 min (south to the left) 60 km from western boundary of domain and in frame of reference moving at $-5\ \mathrm{m\ s^{-1}}$ relative to simulation domain with relative flow vectors shown. Temperature perturbation at intervals of 1 °C also shown.

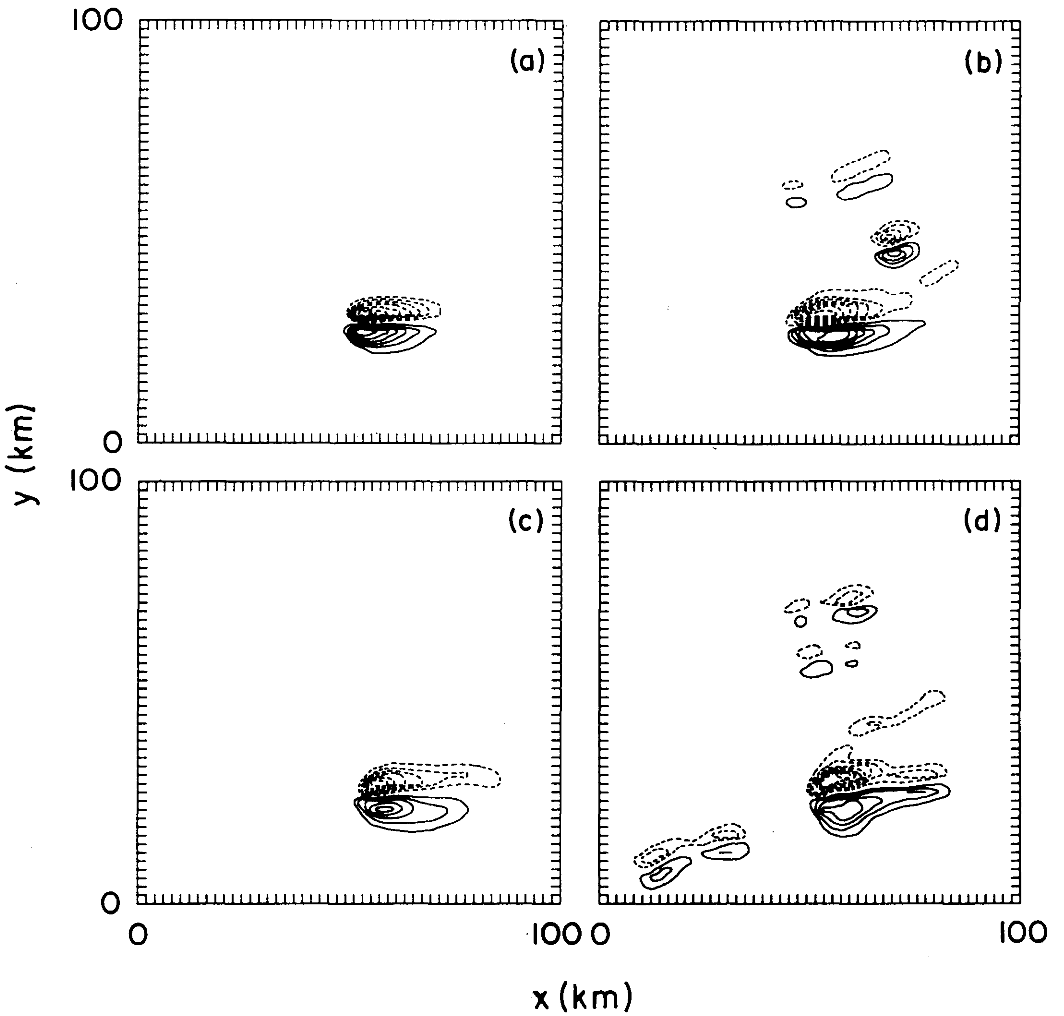

Fig. 13. Vertical component of relative vorticity. Fields are drawn for (a) 120 min at 485 mb, (b) 120 min at 635 mb, (c) 135 min at 485 mb, (d) 135 min at 635 mb. Contour interval $10^{-3}\ s^{-1}$ with zero contour omitted. Positive (negative) values denoted by continuous (broken) contours.

shows that the cold air pool in the Munich storm simulation consisted of air from two families of trajectories. First, a "gravity wave" that does not overturn trajectories (Fig. 11 a–c). Second, an "overturning jump" that is a shallow counterpart of that in Moncrieff and Miller (1976) and in which trajectories overturn and undergo an overall vertical displacement (Fig. 11 d–f). The third space dimension allows such behaviour to occur. There are similarities to the downdraught behaviour during the first several hours of the two-dimensional simulation of Crook and Moncrieff (1988). Figs. 13 and 16 of that paper show a predominant steering level updraught, a forward-directed anvil outflow and a weak downdraught. Moreover, a "gravity wave without stagnation" in the cold pool was identified with an approximately zero net vertical displacement of trajectories that is reminiscent of the wave-like behaviour within the Munich storm simulation. Downdraughts in a convective system that has a prominent forward-directed anvil and which fail to establish a density current but advect through the system without stagnation was reported in Fankhauser et al. (1992). Note

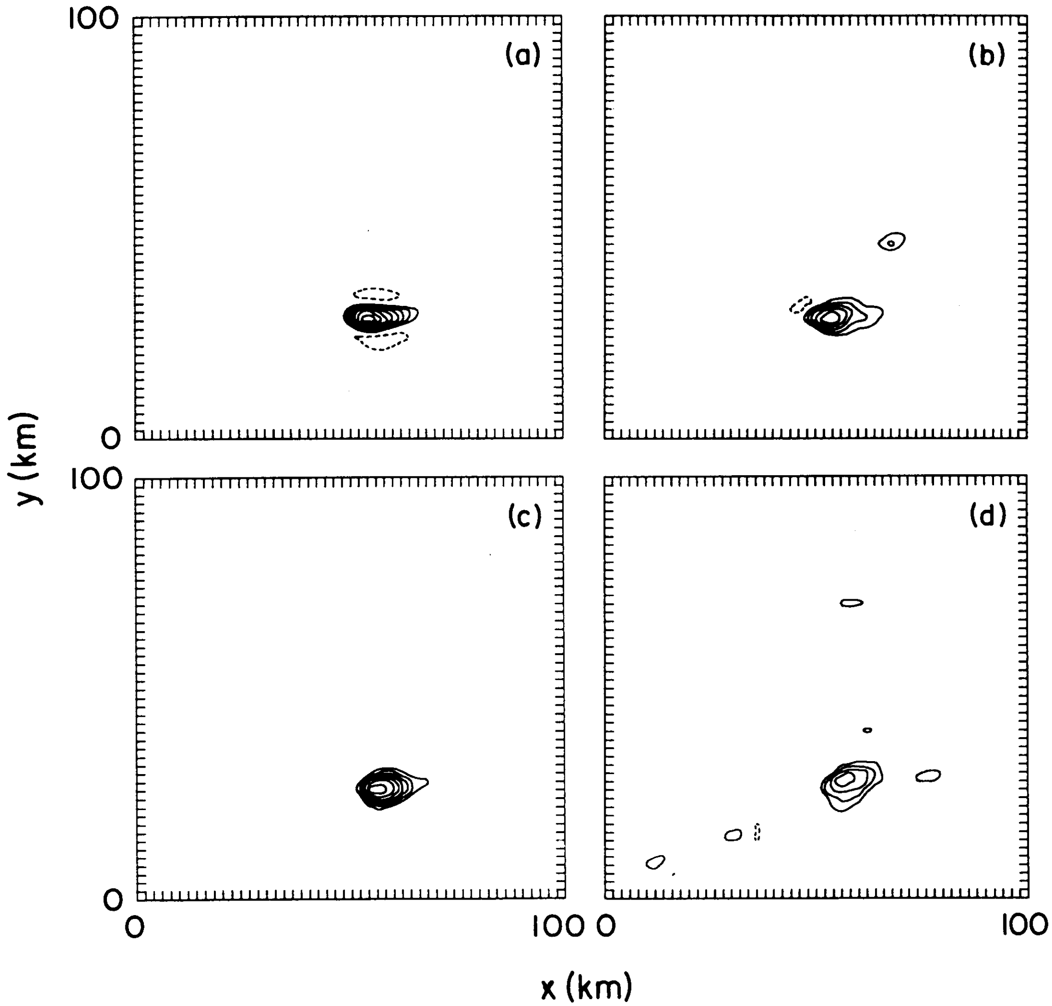

Fig. 14. Vertical component of velocity at: (a) 120 min at 485 mb, (b) 120 min at 635 mb, (c) 135 min at 485 mb, (d) 135 min at 635 mb. Contour interval 2 m s^{-1} with zero contour omitted. Continuous (broken) contours denote ascent (descent).

that a "solitary wave" behaviour constituted the downdraught in one of the squall line simulations in Dudhia et al. (1987) although in that case the anvil outflow was directed rearwards. Overturning of downdraught trajectories originating from ahead of the storm and from beneath the inversion promotes the thermodynamic modification of the boundary and surface layers because air of lower θ_e is deposited near ground level. In contrast, wavelike motion causes small net vertical displacement of trajectories and a minimal surface change in θ_e. In this sense, the jump downdraught in the Munich storm simulation has a similar effect on the boundary layer as that in the tropical squall line study of Miller and Betts (1977; Fig. 9).

A density current circulation does form in the north–south section perpendicular to the direction of travel of the storm system. This behaviour is identified in Fig. 12 which is a vertical cross section extending up through the cold pool and intersecting the zone of maximum convergence located some 60 km from the western boundary of the domain. This figure depicts flow in the frame of reference moving at the southward speed

($-5\,\mathrm{m\,s^{-1}}$) of the density current averaged between 90 and 150 min. Two features are three-dimensional counterparts of properties usually associated with two-dimensional models. First, the maximum convergence at the southern boundary of the density current and the consequent forcing of a secondary convective cell (Thorpe et al., 1982). Second, the vertical shear ($\partial v/\partial y$) in this plane may promote deep lifting of low level air (Rotunno et al., 1988) and convection initiation. On the other hand, the shear at the northern boundary of the cold pool is in the opposite sense and fails to produce robust cell development (note that shear is independent of the coordinate transformation). The combination of these two factors preferentially enhances development of the new cells and storm splitting at the southern rather than the northern boundary of the cold pool. The density current front is aligned parallel and not perpendicular to the direction of storm propagation. This contrasts with the orientation associated with squall lines and thereby distinguishes the dynamics of the storm simulation.

4.5. Rotation

A hypothesis for the maintenance of convection, appropriate when downdraughts are weak, was suggested by Weisman and Bluestein (1985). This involves organised vertical vorticity generation and its role in maintaining a vertical pressure gradient and a vertical acceleration. The vertical component of the relative vorticity in the simulation was analysed. It was found that the only significant organised vorticity signature was a vortex doublet (Fig. 13) clearly produced by the tilting of ambient of horizontal vorticity by the updraught (Fig. 14). It follows that vortex tilting, $(\partial u/\partial z - \partial w/\partial x)\,\partial w/\partial y$, is the dominant term in the vorticity equation. This is a common feature in three-dimensional convection and is distinct from the organised vorticity signature associated with rotating storms (Weisman and Bluestein, 1985; Fig. 7) and with substantial directional shear in the lower troposphere. The vertical shear and horizontal convergence (largely $\partial v/\partial y$) interactions with the cold pool (see Fig. 12), not rotational effects, are the principal mechanisms that force secondary convective cells. Consequently, rotational effects contribute negligibly to the low pressure perturbation above the cold pool and to the vertical pressure gradient in the simulation herein.

5. Conclusions

An extensive series of two-dimensional numerical experiments (not reported herein) failed to produce a convective system that adequately resembled the Munich storm in its multicell stage. Three-dimensionality was essential, despite the low-level turning of the wind with height being small compared to that typical of severe convective storms. Nevertheless, certain qualitative dynamical similarities to two-dimensional convective systems are evident. In particular, the Munich storm travelled in an environment having the shear concentrated in the lower troposphere with a weak mean wind shear above 585 mb and had a prominent steering-level updraught. Idealisations of this type of wind profile have previously been found to promote the initiation of persistent organised convection in two spatial dimensions (e.g., Thorpe et al., 1982; Rotunno et al., 1988; Crook and Moncrieff, 1988; Fovell and Ogura, 1989; Lafore and Moncrieff, 1989). However, the prominent feature of the storm simulation was its right-moving and splitting behaviour, in agreement with observations of the pre-supercell stage of the real Munich storm (Höller and Reinhardt, 1986). This aspect was particularly evident in the rainfall and vertical motion fields (Figs. 6, 7). The low level convergence was maximised at the southeast side of the cold pool which was maintained by shallow downdraughts approaching from the east, in a frame of reference moving with the storm. The density current circulation, the convergence and the vertical shear at the south side of the cold pool cause cell development in this location.

There is an important difference between the simulation and squall lines because a surface stagnation point, a surface convergence maximum and a density current circulation, are confined to a plane perpendicular to the travel direction instead of in a it parallel plane as commonly found in squall lines. This necessitates three spatial dimensions and helps initiate new cells to the right of the storm propagation direction by the mechanism of enhanced dynamical lifting promoted by the vertical shear. In parallel cross section, the overturning propagating jump downdraught behaviour demonstrates a mechanism by which shallow low-energy downdraughts can cause a significant change in θ_e at the surface. These aspects demonstrate a subtle distinction between two- and three-dimensional behaviour.

According to Höller and Reinhardt (1986), during its severe stage, the Munich storm resembled a supercell although in the earlier stages multicell behaviour was evident. The simulation did not produce a supercell storm and it is interesting to speculate on why this was the case. Although one of the cells could indeed have evolved into a supercell (the duration of the run was too short for this to be achieved), there are more compelling basic reasons for the disparity, namely the form of the ambient wind profile. The 1800 GMT wind hodograph for Munich shown on Fig. 2 is quite different from that taken at Payerne at 1200 GMT, the latter being used in the model initial conditions. (The Munich sounding was not used because it is coincident with the storm occurrence and could easily have been modified by this proximity.) However, the straight lower-tropospheric hodograph at Payerne differs considerably from the distinct directional shear in the Munich hodograph (Fig. 2). It is known that straight hodographs promote multicell storms, whereas supercell hailstorms are associated more with directional shear (Chisholm and Rennick, 1972; Browning, 1977).

The Munich storm was not only of rare severity for European storms but modelling has demonstrated that its dynamical structure, particularly that of the downdraughts and cold pool, was somewhat unusual for mid-latitude storms. Convective storms featuring robust rear-to-front cloud and mesoscale downdraughts have dominated attention in the literature. The type of downdraught and secondary cell initiation evident in the simulation is not typical and is probably a result of the strong low-level relative flow.

The simulation has revealed several interesting structural features. A more detailed study using a much larger domain and enhanced resolution is necessary to further investigate a complex life cycle over a period of many hours. A life cycle study of this system is a formidable scientific and computational problem because it spans transitions from initial development in which the role of complex orography may be important, through the multicell stage to a supercell hailstorm, and ultimately to a mesoscale convective complex that probably involves synoptic-scale motion.

6. Acknowledgements

We thank M. Kurz of the Deutscher Wetterdienst for supplying the synoptic and upper air data. R. B. would also like to thank Damon So and colleagues at Imperial College for helpful discussions. The computations were carried out on a CRAY 1S at the University of London Computer Centre.

REFERENCES

Berz, G. 1984. Hagel. *Münchener Rückversicherungs-Gesellschaft.*

Browning, K. A. 1977. The structure and mechanisms of hailstorms. *Met. Monog. 16*, 1–43.

Chisholm, A. J. and Rennick, J. H. 1972. *The kinematics of multicell and supercell Alberta hailstorms.* Research Council of Alberta Hail Studies Rep. no. 72-2, 24–31.

Crook, N. A. and Moncrieff, M. W. 1988. The effect of large-scale convergence on the generation and maintenance of deep moist convection. *J. Atmos. Sci. 45*, 3606–3624.

Dudhia, J. and Moncrieff, M. W. 1989. Three-dimensional simulation of an Oklahoma squall line with right-flank supercells. *J. Atmos. Sci. 46*, 3363–3391.

Dudhia, J., Moncrieff, M. W. and So, D. W. K. 1987. The two-dimensional dynamics of West African squall lines. *Quart. J. Roy. Met. Soc. 113*, 121–146.

Fankhauser, J. C., Barnes, G. M. and LeMone, M. A. 1992. Structure of a midlatitude squall line formed in unidirectional shear. *Mon. Wea. Rev. 120*, 237–260.

Fovell, R. G. and Ogura, Y. 1989. Effect of vertical wind shear on numerically simulated multicell storm structure. *J. Atmos. Sci. 46*, 3144–3176.

Heimann, D. and Kurz, M. 1985. The Munich Hailstorm of 12 July 1984: A discussion of the synoptic situation. *Beitr. Phys. Atmosph. 58*, 528–544.

Höller, H. and Reinhardt, M. 1986. The Munich hailstorm of 12 July 1984: Convective development and preliminary hailstone analysis. *Beitr. Phys. Atmosph. 59*, 1–12.

Klemp, J. B. and Wilhelmson, R. B. 1978. Simulations of right- and left-moving storms produced through storm splitting. *J. Atmos. Sci. 35*, 1097–1110.

Kurz, M. 1985. Zum Münchener Hagelunwetter vom 12.07.1984. *Meteorol. Rdsch. 38*, 129–144.

Lafore, J.-P. and Moncrieff, M. W. 1989. A numerical investigation of the organization and interaction of the convective ans stratiform regions of tropical squall lines. *J. Atmos. Sci. 46*, 521–544.

Maddox, R. A. 1980. Mesoscale convective systems. *Bull. Amer. Meteor. Soc. 61*, 1374–1387.

Miller, M. J. 1978. The Hampstead storm: A numerical simulation of a quasi-stationary cumulonimbus system. *Quart. J. Roy. Meteor. Soc. 104*, 413–427.

Miller, M. J. and Betts, A. K. 1977. Traveling convective storms over Venezuela. *J. Atmos. Sci. 105*, 833–848.

Miller, M. J. and Pearce, R. P. 1974. A three-dimensional primitive equation model of cumulonimbus convection. *Quart. J. Roy. Meteor. Soc. 100*, 133–154.

Moncrieff, M. W. 1978. The dynamical structure of two-dimensional steady convection in constant vertical shear. *Quart. J. R. Meteor. Soc. 104*, 563–567.

Moncrieff, M. W. 1981. A theory of organised steady convection and its transport properties. *Quart. J. R. Meteor. Soc. 107*, 29–50.

Moncrieff, M. W. and Green, J. S. A. 1972. The propagation and transfer properties of steady convective returning in shear. *Quart. J. Roy. Meteor. Soc. 98*, 336–352.

Moncrieff, M. W. and Miller, M. J. 1976. The dynamics and simulation of tropical cumulonimbus and squall lines. *Quart. J. Roy. Meteor. Soc. 102*, 373–394.

Rotunno, R., Klemp, J. B. and Weisman, M. L. 1988. A theory for strong, long-lived squall lines. *J. Atmos. Sci. 45*, 463–485.

Thorpe, A. J. and Miller, M. J. 1978. Numerical simulations showing the role of the downdraught in cumulonimbus motion and splitting. *Quart. J. R. Meteor. Soc. 104*, 873–893.

Thorpe, A. J., Miller, M. J. and Moncrieff, M. W. 1982. Two-dimensional convection in non-constant shear: A model of mid-latitude squall lines. *Quart. J. Roy. Meteor. Soc. 108*, 739–762.

Weisman, M. L. and Klemp, J. B. 1984. The structure and classification of numerically simulated convective storms in directionally varying wind shears. *Mon. Wea. Rev. 112*, 2479–2498.

Weisman, M. L. and Bluestein, H. B. 1985. Dynamics of numerically simulated low precipitation storms. Preprint Volume, *14th Conf. Severe Local Storms*, Amer. Meteor. Soc., 167–170.

Printed in Belgium